CRYSTAL GROWTH & DESIGN

pubs.acs.org/crystal Article

Crystal Phase, Electronic Structure, and Surface Band Bending of $(In_xGa_{1-x})_2O_3$ Alloy Wide-Band-Gap Semiconductors

Zhenni Yang,[#] Wenshan Chen,[#] Siliang Kuang, Ziqian Sheng, Jueli Shi, Duanyang Chen, Meiyan Cui, Hongji Qi,* and Kelvin H. L. Zhang*

Cite This: Cryst. Growth Des. 2022, 22, 7325−7330

Read Online

ACCESS | Metrics & More | Article Recommendations

Downloaded via XIAMEN UNIV on January 20, 2023 at 08:59:09 (UTC).
See https://pubs.acs.org/sharingguidelines for options on how to legitimately share published articles.

ABSTRACT: Ga_2O_3 is emerging as a promising wide-band-gap semiconductor for high-power electronics and deep ultraviolet optoelectronics. Alloying Ga_2O_3 with In_2O_3 leads to the modulation of the band gaps and possible carrier confinement achieved at the heterointerface. In this work, we report a systematic study on the crystallographic phase, electronic structure, and surface band bending of $(In_xGa_{1-x})_2O_3$ thin films over the whole composition range of $0 \leq x \leq 1$ grown on α-Al_2O_3 (0001) substrates by pulsed laser deposition. It was found that with In content $x < 0.2$, a monoclinic β-phase of an $(In_xGa_{1-x})_2O_3$ film is epitaxially grown on Al_2O_3 (0001), while a bixbyite phase of the $(In_xGa_{1-x})_2O_3$ film grows when $x \geq 0.8$. When $0.2 \leq x < 0.8$, a mixed β-phase and bixbyite phase coexist. The evolution of electronic structures of the $(In_xGa_{1-x})_2O_3$ films was examined by high-resolution X-ray photoemission spectroscopy (XPS) and optical absorption spectroscopy. For the β-phase films, the optical band gaps decrease from 4.96 eV for Ga_2O_3 to 4.43 eV for $x = 0.4$, while for bixbyite $(In_xGa_{1-x})_2O_3$, the optical band gaps slightly increase from 3.57 eV for In_2O_3 to 3.70 eV for $x = 0.8$. Detailed electronic structure study indicates that the decrease of band gaps of $(In_xGa_{1-x})_2O_3$ with an increase of In content mainly results from the upper movement of the valence band edge because the shallow In 4d orbitals introduce a hybridized state with O 2p at the top of the valence band. In addition, the presence of surface electron accumulation (*i.e.*, downward band bending) was identified at the surface region of the $(In_xGa_{1-x})_2O_3$ films with $x \geq 0.6$, which would provide an opportunity to modulate the surface electronic properties for device applications.

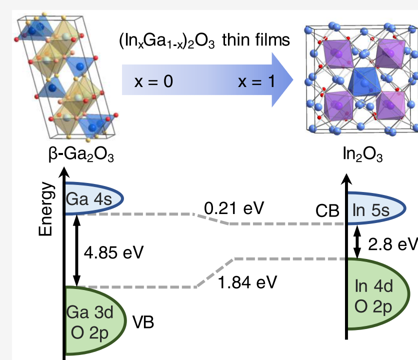

1. INTRODUCTION

Group-III sesquioxides In_2O_3 and Ga_2O_3 are wide-band-gap semiconductors, which hold great promise for applications in the fields of optoelectronics and power electronics.[1−4] On the one hand, In_2O_3 has an optically forbidden band gap of ∼ 2.8 eV, with strong optical absorption occurring from valence bands nearly 1 eV below the valence band maximum (VBM), resulting in the onset of strong optical absorption at around 3.6 eV.[5,6] This property renders In_2O_3 highly transparent in the visible regime. Meanwhile, In_2O_3 doped with Sn (*aka* ITO) can significantly increase the electrical conductivity. ITO is the most widely used transparent conducting oxide with applications in flat panel displays, solar cells, and electrochromic devices.[7,8] On the other hand, Ga_2O_3 has been rapidly emerging as the most potential wide-band-gap semiconductor of 4.85 eV for applications in solar-blind ultraviolet (UV) photodetectors, high-power electronic devices, and deep UV transparent conductive electrodes in recent years.[9−12] Furthermore, the two oxide semiconductors share quite a similar electronic structure. The valence bands (VBs) of In_2O_3 and Ga_2O_3 are mainly composed of the filled O $2p^6$ derived state, while the conduction band (CB) is formed primarily by the empty In 5s or Ga 4s states. The In 5s and Ga 4s orbitals are spherical in shape and spatially extended, which can overlap extensively with neighboring s orbitals. Such extensive orbital overlapping provides a facile pathway for the conduction of electrons. Alloying In_2O_3 with Ga_2O_3 will offer a way to modulate the band gaps and also other material properties and to construct heterojunctions to enable electronic modulation to fully exhaust their potential to facilitate the development of electronic devices.[13,14]

However, a major issue is that In_2O_3 and Ga_2O_3 possess different crystalline structures. The solubility between In_2O_3 and Ga_2O_3 is limited, and therefore phase segregation is expected for $(In_xGa_{1-x})_2O_3$ alloys. In_2O_3 has two polymorphs: cubic bixbyite (space group $Ia\bar{3}$) and corundum (space group $R\bar{3}c$). The cubic bixbyite In_2O_3 (Figure 1a) is the most thermodynamically stable structure. Ga_2O_3 has five polymorphs, in which the monoclinic β-phase structure (space

Received: August 22, 2022
Revised: October 19, 2022
Published: October 31, 2022

ACS Publications © 2022 American Chemical Society

https://doi.org/10.1021/acs.cgd.2c00948
Cryst. Growth Des. 2022, 22, 7325−7330

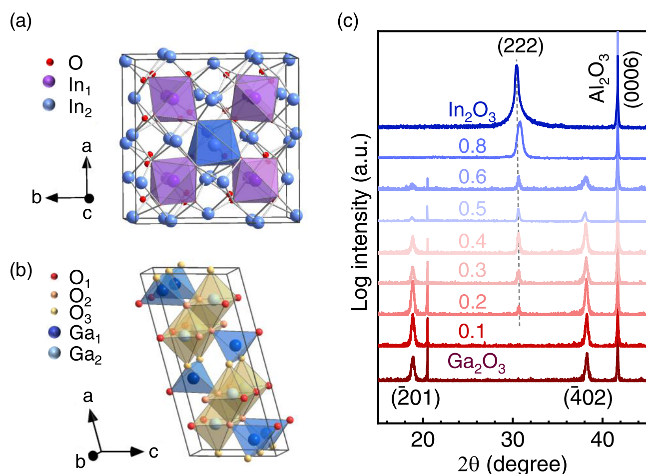

Figure 1. Crystal structure of (a) bixbyite In_2O_3 and (b) monoclinic β-Ga_2O_3. (c) XRD θ−2θ scans of $(In_xGa_{1-x})_2O_3$ ($0 \leq x \leq 1$) thin films grown on α-Al_2O_3 (0001) substrates.

group $C2/m$) is the most stable one. The crystal structure of β-phase Ga_2O_3 (Figure 1b) has two inequivalent Ga sites, including a distorted tetrahedrally (T_d) coordinated Ga_1 site and a distorted octahedrally (O_h) coordinated Ga_2 site. It is of interest to understand what crystalline structure the alloys will adopt in the $(In_xGa_{1-x})_2O_3$ alloys as a function of composition and how the different structures influence the optical and electronic properties. Edwards et al. established the phase diagram of $(In_xGa_{1-x})_2O_3$ alloys using polycrystalline powders synthesized by solid-state synthesis.[15] They found that the solubility of In_2O_3 in Ga_2O_3 with a monoclinic β-phase structure is limited at $x = 0.44$, while for the cubic bixbyite In_2O_3, the solubility limit for Ga is only at $x = 0.9$. In the composition range of $0.4 < x < 0.9$, the samples are biphasic, consisting of mixed phases of Ga-doped cubic In_2O_3 and In-doped monoclinic β-Ga_2O_3. Thin films of $(In_xGa_{1-x})_2O_3$ have been grown by different techniques such as MOCVD, PLD, MBE, and so on, but the reported values of solubility are quite scattered, depending on the growth techniques and growth parameters. Oshima and Fujita grew β-phase $(In_xGa_{1-x})_2O_3$ films on β-Ga_2O_3 layer-buffered Al_2O_3 (0001) *via* MBE.[16] The films maintained a monoclinic crystal structure up to $x = 0.35$. However, the crystalline quality degraded with an increase in indium content, such that films with $x = 0.35$ were amorphous. Swallow et al. studied the phase and electronic structure of $(In_xGa_{1-x})_2O_3$ films grown by PLD and found the In content (x) is low to maintain the monoclinic β-phase, while a hexagonal structure mixed with monoclinic and bixbyite phases is present when $0.35 < x < 0.7$.[17] Meanwhile, the indium incorporation into Ga_2O_3 causes a significant reduction in the band gap.

Though previous works have reported the solubility, crystal structures, and band gaps of the $(In_xGa_{1-x})_2O_3$ alloys, it has not been explored yet how the epitaxial relationship and the evolution of the electronic structures of the $(In_xGa_{1-x})_2O_3$ alloying thin films as a function of In contents. This fundamental knowledge is crucial to the development of optoelectronic devices. In this work, we provide an in-depth study of the epitaxial growth of $(In_xGa_{1-x})_2O_3$ thin films over the whole composition range of $0 \leq x \leq 1$ on Al_2O_3 (0001) substrates grown by PLD. The evolution of the electronic structures was studied by XPS at the VB and core level spectra. The results, in combination with optical spectroscopy and transport measurement, allow us to determine the change of the electronic structures, surface band bending, and energy band alignment between In_2O_3 and Ga_2O_3 over the whole composition range.

2. EXPERIMENTAL DETAILS

2.1. Thin-Film Growth. $(In_xGa_{1-x})_2O_3$ thin films with a thickness of 160 nm were grown on Al_2O_3 (0001) substrates by PLD. The $(In_xGa_{1-x})_2O_3$ targets were prepared from Ga_2O_3 and In_2O_3 powders (99.999%, Alfa Aesar) by grinding, pressing, and sintering at 1350 °C in the air for 24 h. The In content (x) in $(In_xGa_{1-x})_2O_3$ films is the nominal In mole ratio used for target preparation. Laser ablation was performed with an energy density of 1.5 J cm^{-2} and a repetition rate of 5 Hz with a 248 nm KrF excimer laser. The deposition temperature was 650 °C, and oxygen partial pressure was set at 10 mTorr during growth.

2.2. Characterizations. The epitaxial relationship and crystal structure were examined by X-ray diffraction (XRD) using a PANalytical four-circle diffractometer. X-ray reflectivity (XRR) was used to measure the film thickness. Atomic force microscopy (AFM) was used to characterize the surface morphology. Optical absorption spectroscopy was measured at room temperature using a Cary 5000 spectrophotometer. The film compositions and electronic structures were measured by high-resolution XPS using a laboratory monochromatic Al Kα_1 X-ray ($h\nu$ = 1486.6 eV) at normal emission (electron take-off angle = 90° relative to the surface plane). The binding energy (BE) was calibrated by an Au foil placed in electrical contact with the film surface. The XPS energy resolution was 0.5 eV. The electrical properties of the films were characterized using Hall measurement in a van der Pauw 4-point configuration at room temperature. Ohmic contact pads with a metal stack of 5 nm Ni/100 nm Au were deposited by magnetron sputtering at the corners of the rectangular samples.

3. RESULTS AND DISCUSSION

3.1. Thin-Film Growth. Figure 1c shows the out-of-plane XRD patterns of the $(In_xGa_{1-x})_2O_3$ films over the whole composition range collected by θ−2θ scans. The crystal structure gradually changes from monoclinic β-Ga_2O_3 to bixbyite In_2O_3 with an increase in In content. For In content $x < 0.2$, the monoclinic β-films are epitaxially grown on α-Al_2O_3 (0001) substrates. Bragg peaks corresponding to ($\bar{2}$01) and ($\bar{4}$02) reflections of Ga_2O_3 can be observed at 18.89° and 38.28°, respectively, indicating the out-of-plane epitaxial relationship of Ga_2O_3 ($\bar{2}$01)||Al_2O_3 (0001). However, with an increase in In content, an extra peak emerges at ∼30.6°, corresponding to the reflection from the bixbyite In_2O_3 (222) plane. This indicates the phase segregation of In_2O_3 because of the low solubility limit of In_2O_3 in Ga_2O_3. Previous work reported that the epitaxial $(In_xGa_{1-x})_2O_3$ films have solubility values of $x < 0.35$ grown by MBE and $x < 0.20$ grown by PLD.[16,18]

It can be noticed that the Bragg peak of the ($\bar{4}$02) reflection from the β-phase $(In_xGa_{1-x})_2O_3$ shifts to smaller angles with an increase in In content, suggesting the increase of out-of-plane lattice constants from 5.825 Å for Ga_2O_3 to 5.858 Å for $(In_{0.6}Ga_{0.4})_2O_3$ (see Figure 2a) because of the larger ionic radius of In^{3+} (0.79 Å) than that of Ga^{3+} (0.62 Å). The larger indium cations prefer to occupy the octahedron site of the monoclinic structure. In addition, the bixbyite structure also exhibits a decrease of out-of-plane lattice constants with increasing content of Ga, *e.g.*, 10.171 Å for In_2O_3 and 10.106 Å for $(In_{0.2}Ga_{0.8})_2O_3$. AFM images were collected to investigate the film morphology. Figure 2b shows the AFM images of β-

https://doi.org/10.1021/acs.cgd.2c00948
Cryst. Growth Des. 2022, 22, 7325−7330

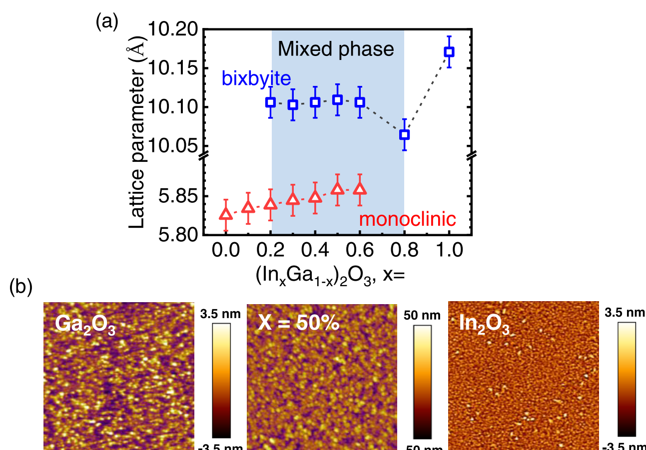

Figure 2. (a) Out-of-plane lattice parameters of bixbyite In_2O_3 (blue rectangle) and monoclinic β-Ga_2O_3 (red triangle) in the $(In_xGa_{1-x})_2O_3$ ($0 \leq x \leq 1$) system as a function of indium content. (b) AFM images of the Ga_2O_3, $(In_{0.5}Ga_{0.5})_2O_3$, and In_2O_3 with a scan area of 5 × 5 μm^2, respectively.

Ga_2O_3, $(In_{0.5}Ga_{0.5})_2O_3$, and In_2O_3 thin films (x = 0, 0.5, and 1), respectively. It is found that the as-grown thin films with a single phase (x = 0 and 1) present a quite smooth surface with a small root-mean-square (RMS) roughness of ~1 nm. While for the $(In_xGa_{1-x})_2O_3$ alloys with phase segregation, a granular structure with small three-dimensional islands is observed.

To determine the epitaxial relationship between the $(In_xGa_{1-x})_2O_3$ thin films and Al_2O_3, we also performed phi scans of Ga_2O_3 ($\bar{4}01$), In_2O_3 (440), and Al_2O_3 ($11\bar{2}6$) planes in Figure 3a. For the β-Ga_2O_3 thin film, six strong diffraction peaks separated by 60° are observed, which originate from the presence of a sixfold in-plane rotational symmetry. Moreover, it can be interpreted as the double effect of the twofold in-plane rotational symmetry of monoclinic β-Ga_2O_3 and three kinds of equivalent growth directions of Ga_2O_3 on the Al_2O_3 (0001) surface.[19,20] Figure 3b schematically illustrates the atomic position relation between the unit cell of monoclinic β-Ga_2O_3 and that of α-Al_2O_3 and the top-view projected geometrical epitaxial relationship of Ga_2O_3 ($\bar{2}01$)||Al_2O_3 (0001) with Ga_2O_3 [010]||Al_2O_3 [$1\bar{1}00$]. The Ga_2O_3 ($\bar{2}01$) plane consists of distorted cubic close packing of O anions with octahedral GaO_6 and tetrahedral GaO_4. The lattice mismatch between β-Ga_2O_3 ($\bar{2}01$) and α-Al_2O_3 (0001) is ~6.6%.[21−23] As shown in Figure 3b, good epitaxial growth can be maintained because the O atoms in the Ga_2O_3 ($\bar{2}01$) plane share a very similar arrangement with those of the Al_2O_3 (0001) plane.[22,24]

For bixbyite In_2O_3, (111) oriented films are grown on Al_2O_3 (0001). The phi scan of the In_2O_3 film shown in Figure 3a indicates a sixfold in-plane symmetry, resulting from the register of the In_2O_3 (111) plane with the sixfold Al_2O_3 (0001) plane.[25] Figure 3c illustrates the epitaxial relationship of In_2O_3 (111) on Al_2O_3 (0001), with In_2O_3 [$\bar{1}10$] ||Al_2O_3 [$\bar{1}010$] and In_2O_3 [$\bar{1}\bar{1}2$]||Al_2O_3 [$\bar{1}2\bar{1}0$]. There is a large lattice mismatch of −13.2% between In_2O_3 and Al_2O_3. However, it has been shown that the large mismatch between In_2O_3 and Al_2O_3 can be accommodated by the domain match epitaxy (DME) mechanism, in which eight planes of In_2O_3 ($1\bar{1}0$) match with seven planes of Al_2O_3 ($10\bar{1}0$).[6] The DME mechanism can effectively reduce the mismatch from −13.2% to a residual mismatch of −0.8% and thereby give rise to the epitaxial growth of the In_2O_3 (111) film on Al_2O_3.

3.2. Electrical and Optical Properties. The optical band gaps of the $(In_xGa_{1-x})_2O_3$ thin films can be calculated *via* the *Tauc* plots, as shown in Figure 4a and the inset. For the monoclinic structure (x < 0.2), the optical band gap monotonically decreases with the introduction of In, *e.g.*, the value decreases from 4.96 eV for β-Ga_2O_3 to 4.43 eV for x = 0.4. When x > 0.5, the $(In_xGa_{1-x})_2O_3$ films convert into the bixbyite structure with band gaps of 3.6−3.7 eV.

Figure 4b shows the Hall mobility (μ) and carrier concentration (n_e) of the $(In_xGa_{1-x})_2O_3$ thin films as a function of In content (x) measured by Hall measurements. The films with $x \leq 0.1$ do not show measurable conductivity. Both the carrier concentration and mobility increase with the content of In. Specifically, the Hall mobility increases from 1.8 cm^{-1} V^{-1} s^{-1} for x = 0.2 to 57.9 cm^{-1} V^{-1} s^{-1} for In_2O_3, and

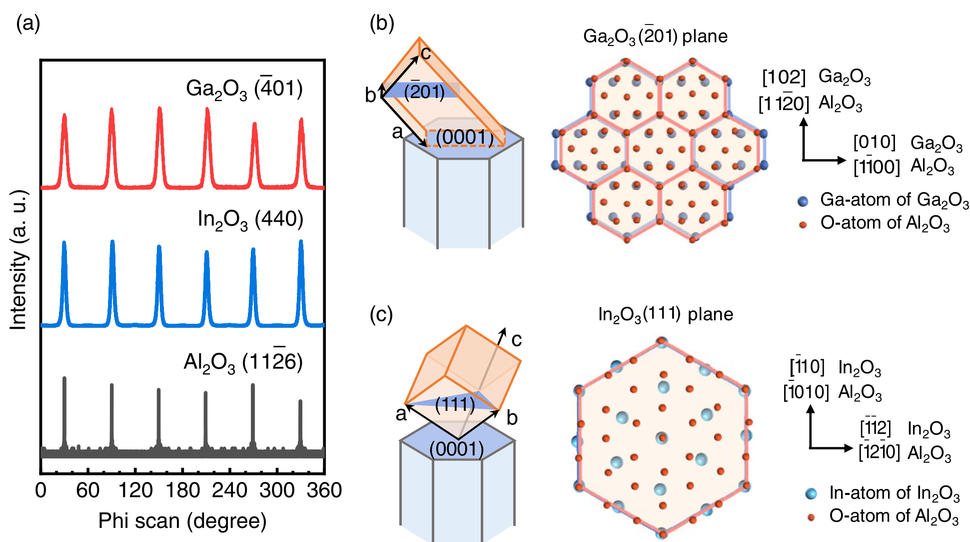

Figure 3. (a) XRD phi scans of the ($\bar{4}01$) reflection of β-Ga_2O_3 and the (440) reflection of In_2O_3 thin films grown on α-Al_2O_3 (0001) substrates. Schematic diagrams of the epitaxial relationship between (b) β-Ga_2O_3 ($\bar{2}01$), (c) In_2O_3 (111), and Al_2O_3 (0001) planes. β-Ga_2O_3 ($\bar{2}01$) and In_2O_3 (111) are parallel to Al_2O_3 (0001).

https://doi.org/10.1021/acs.cgd.2c00948
Cryst. Growth Des. 2022, 22, 7325−7330

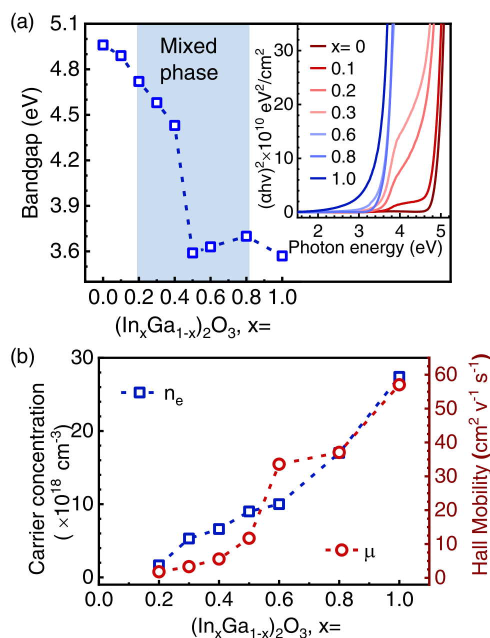

Figure 4. (a) Optical band gaps of $(In_xGa_{1-x})_2O_3$ thin films as a function of In content x. The insert picture is the *Tauc* plot of $(\alpha h\nu)^2$ vs $h\nu$ for the extrapolation of band gaps of $(In_xGa_{1-x})_2O_3$ films. (b) Carrier concentration (blue rectangle) and Hall mobility (red circle) of $(In_xGa_{1-x})_2O_3$ thin films as a function of In content x.

the corresponding carrier concentrations increase from 1.64 × 10^{18} cm^{-3} to 2.74 × 10^{19} cm^{-3}.

3.3. Evolution of the Electronic Structure and Surface Properties.

Figure 5a displays the XPS VB spectra of

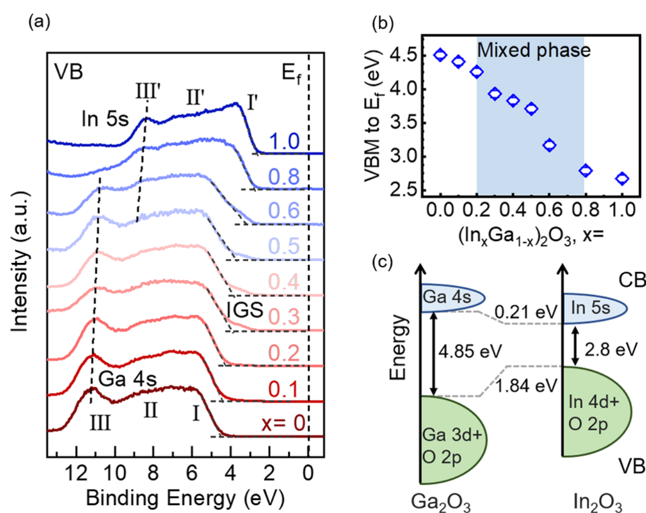

Figure 5. (a) Valence band XPS spectra of the $(In_xGa_{1-x})_2O_3$ thin film with different indium contents. (b) Energy positions of the valence band edge from XPS referenced to E_f about $(In_xGa_{1-x})_2O_3$ thin films as a function of x. (c) Schematic electronic structures of Ga_2O_3 and In_2O_3.

$(In_xGa_{1-x})_2O_3$ alloys. All of the XPS spectra are referenced to the Fermi level (E_f) as zero energy. The VB of Ga_2O_3 exhibits three main regions marked as "I", "II", and "III" at a BE range of 5−13 eV, attributed to the occupied O $2p^6$ states with minor hybridization with Ga 3d at region I, Ga 4p at region II, and Ga 4*s* at region III.[26,27] Similarly, the VB of In_2O_3 primarily consists of filled O $2p^6$ states with a minor contribution from hybridized states with In 4d at region I', In 5p at region II', and In 5s states at region III'.[28,29] We determined the VBM positions relative to the E_f by linear extrapolation of the leading edge of the VB to the baseline. Figure 5b shows the VBM to E_f separations as a function of the In content. The VBM position for Ga_2O_3 is located at ∼4.5 eV below the E_f, whereas the VBM position for In_2O_3 is at ∼ 2.7 eV below the E_f. For the β-phase $(In_xGa_{1-x})_2O_3$ ($x \leq 0.2$) films, the VBM gradually moves to lower binding energy with an increase in In content. However, when $x \geq 0.3$ (mixed phase), a new in-gap state (as marked as IGS) emerges at a binding energy range of 3−4 eV. The in-gap state is attributed to the electronic state from the top of VB of In_2O_3 since its intensity increases with the increase in In contents. This is consistent with XRD results showing phase separation at $x \geq 0.3$. In another word, the VB spectra for the mixed-phase films are the combination of VBs of β-phase and bixbyite $(In_xGa_{1-x})_2O_3$. With a further increase in In content to more than 0.8, the bixbyite phase is reached, and the VB structure is close to that of In_2O_3.

The above-mentioned detailed analysis of the change of VB spectra reveals important insights into the evolution of electronic structures of the $(In_xGa_{1-x})_2O_3$ system and the band alignment between Ga_2O_3 and In_2O_3. The fundamental band gaps decrease from 4.85 eV for Ga_2O_3 to 2.8 eV for In_2O_3. The decrease of the band gap arises from the relative energy difference between the VB edge and CB edge. It is important to know the respective contribution of the change of the VB edge and the CB edge. Figure 5c presents the schematic energy diagrams for the electronic structures of Ga_2O_3 and In_2O_3. As indicated by the VBM positions for In_2O_3 and Ga_2O_3 from Figure 5a-b, the VBM of In_2O_3 is ∼1.84 eV lower in energy than that of Ga_2O_3. This indicates a VB offset of around 1.84 eV between Ga_2O_3 and In_2O_3 with respect to E_f. Furthermore, considering the fundamental band gaps of In_2O_3 and Ga_2O_3, the CB offset between In_2O_3 and Ga_2O_3 and with respect to E_f is around 0.21 eV (see Figure 5c). Therefore, we can conclude that the decrease in band gaps in the $(In_xGa_{1-x})_2O_3$ system with an increase in the indium content (x) mainly results from the upper movement of the VB edge, while the contribution of the downward movement of the CB edge is relatively small. We ascribe the lower energy of the VBM position for In_2O_3 to the hybridization of In 4d with O 2p at the top of VB. As mentioned above, the top of VB for Ga_2O_3 (region I in Figure 5a) and In_2O_3 (region I' in Figure 5a) is associated with the hybridization state of Ga 3d with O 2p and In 4d with O 2p, respectively. Figure 6a displays the Ga 3d and In 4d semicore levels. In 4d is located at a BE of 17.9 eV, lower than that of Ga 3d at 21.3 eV. The shallower In 4d state would result in more hybridization with O 2p at the top of VB. This is in agreement with recent work by Swallow et al. on the electronic structure of $(In_xGa_{1-x})_2O_3$ alloys predicted by using DFT, which showed a higher In 4d density of state in In_2O_3 than that of Ga 3d in Ga_2O_3.[17]

It has been demonstrated that there is a two-dimensional surface electron accumulation layer (SEAL) existing on the surface region of In_2O_3.[30−32] As shown by the magnified VB spectra around the E_f in Figure 6b, for the bixbyite phase $(In_xGa_{1-x})_2O_3$ with high In contents ($x \geq 0.8$), there is a clear intensity feature across the E_f, which confirms the presence of SEAL on the bixbyite $(In_xGa_{1-x})_2O_3$ films. From Figure 6b, we can determine that the SEAL still exists for the mixed phase

https://doi.org/10.1021/acs.cgd.2c00948
Cryst. Growth Des. 2022, 22, 7325−7330

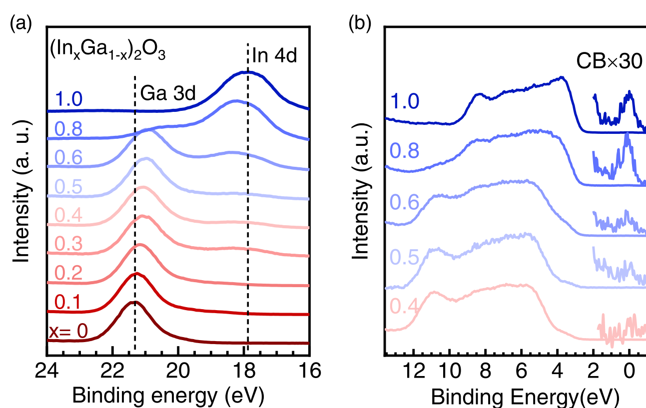

Figure 6. (a) Ga 3d and In 4d core levels and (b) VB spectra with different indium contents. Expansion of the conduction band magnified × 30 for the spectra.

with x = 0.6. The presence of SEAL would introduce a downward band bending at the surface region, which is an important property for the application of In_2O_3 as a gas-sensing material, and it also facilitates the formation of Ohmic contacts while making the formation of Schottky contacts challenging.[33,34] On the other hand, for the β-phase Ga_2O_3, it has been demonstrated that there is an upward band bending existing at the surface region, *i.e.*, the surface electron depletion layer.[35,36] The surface electron depletion layer makes the formation of Ohmic contacts challenging for Ga_2O_3-based power electronic devices. Therefore, the presence of SEAL in the $(In_xGa_{1-x})_2O_3$ system would provide an opportunity to modulate the surface electronic properties for device applications.

4. CONCLUSIONS

In summary, we have studied the epitaxial growth, the evolution of the electronic structure, and surface band bending of the $(In_xGa_{1-x})_2O_3$ thin films over the whole composition range of $0 \leq x \leq 1$ grown on α-Al_2O_3 (0001) substrates. With In content $x < 0.2$, monoclinic β-phase $(In_xGa_{1-x})_2O_3$ films are formed on Al_2O_3 (0001), with an epitaxial relationship of Ga_2O_3 $(\bar{2}01)$||Al_2O_3 (0001). For $x \geq 0.8$, the bixbyite $(In_xGa_{1-x})_2O_3$ films are grown with an epitaxial relationship of *bcc*-In_2O_3 (111)||Al_2O_3 (0001). When $0.2 \leq x < 0.8$, mixed β-phase and bixbyite phase coexist. For the β-phase $(In_xGa_{1-x})_2O_3$ films, the optical band gaps decrease from 4.96 eV for Ga_2O_3 to 4.43 eV for x = 0.4, while for bixbyite films, the optical band gaps slightly increase from 3.57 eV for In_2O_3 to 3.70 eV for x = 0.8. Detailed studies on the electronic structure reveal that the decrease in band gaps in the $(In_xGa_{1-x})_2O_3$ system with an increase in In content primarily results from the upper movement of the VB edge, while the contribution of downward movement of the CB edge is relatively small. The upper movement of the VB edge is caused by the significant hybridization between shallow In 4d orbitals with O 2p at the top of VB. This results in a much shallower valence band edge for In_2O_3 compared with that for Ga_2O_3. Based on the XPS VB spectra, we can infer that In_2O_3 and Ga_2O_3 have valence band and conduction band offsets of 1.84 and 0.21 eV, respectively. In addition, we found the presence of surface electron accumulation (*i.e.*, downward band bending) at the surface region of the $(In_xGa_{1-x})_2O_3$ films with $x \geq 0.6$, which would provide an opportunity to modulate the surface electronic properties for device applications.

AUTHOR INFORMATION

Corresponding Authors

Hongji Qi − *Key Laboratory of Materials for High Power Laser, Shanghai Institute of Optics and Fine Mechanics, Chinese Academy of Sciences, Shanghai 201800, P. R. China; Hangzhou Institute of Optics and Fine Mechanics, Chinese Academy of Sciences, Hangzhou 311421, P. R. China;* Email: qhj@siom.ac.cn

Kelvin H. L. Zhang − *State Key Laboratory of Physical Chemistry of Solid Surfaces, College of Chemistry and Chemical Engineering, Xiamen University, Xiamen 361005, P. R. China;* orcid.org/0000-0001-9352-6236; Email: Kelvinzhang@xmu.edu.cn

Authors

Zhenni Yang − *State Key Laboratory of Physical Chemistry of Solid Surfaces, College of Chemistry and Chemical Engineering, Xiamen University, Xiamen 361005, P. R. China; Hangzhou Institute of Optics and Fine Mechanics, Chinese Academy of Sciences, Hangzhou 311421, P. R. China*

Wenshan Chen − *State Key Laboratory of Physical Chemistry of Solid Surfaces, College of Chemistry and Chemical Engineering, Xiamen University, Xiamen 361005, P. R. China*

Siliang Kuang − *State Key Laboratory of Physical Chemistry of Solid Surfaces, College of Chemistry and Chemical Engineering, Xiamen University, Xiamen 361005, P. R. China; Hangzhou Institute of Optics and Fine Mechanics, Chinese Academy of Sciences, Hangzhou 311421, P. R. China*

Ziqian Sheng − *State Key Laboratory of Physical Chemistry of Solid Surfaces, College of Chemistry and Chemical Engineering, Xiamen University, Xiamen 361005, P. R. China*

Jueli Shi − *State Key Laboratory of Physical Chemistry of Solid Surfaces, College of Chemistry and Chemical Engineering, Xiamen University, Xiamen 361005, P. R. China*

Duanyang Chen − *Key Laboratory of Materials for High Power Laser, Shanghai Institute of Optics and Fine Mechanics, Chinese Academy of Sciences, Shanghai 201800, P. R. China;* orcid.org/0000-0001-8579-3131

Meiyan Cui − *State Key Laboratory of Structural Chemistry, Fujian Institute of Research on the Structure of Matter, Chinese Academy of Sciences, Fuzhou 350002, P. R. China*

Complete contact information is available at: https://pubs.acs.org/10.1021/acs.cgd.2c00948

Author Contributions

#Z.Y. and W.C. contributed equally to this work.

Notes

The authors declare no competing financial interest.

ACKNOWLEDGMENTS

K.H.L.Z. acknowledges funding support from the National Natural Science Foundation of China (Grant Nos. 21872116 and 22075232).

REFERENCES

(1) Yu, X.; Marks, T. J.; Facchetti, A. Metal oxides for optoelectronic applications. *Nat. Mater.* **2016**, *15*, 383−396.

(2) Shi, J.; Zhang, J.; Yang, L.; et al. Wide bandgap oxide semiconductors: from materials physics to optoelectronic devices. *Adv. Mater.* **2021**, *33*, No. 2006230.

(3) Pearton, S. J.; Yang, J.; Cary IV, P. H.; et al. A review of Ga_2O_3 materials, processing, and devices. *Appl. Phys. Rev.* **2018**, *5*, No. 011301.
(4) Von Wenckstern, H. Group-III sesquioxides: Growth, physical properties and devices. *Adv. Electron. Mater.* **2017**, *3*, No. 1600350.
(5) Walsh, A.; Da Silva, J. L.; Wei, S. H.; et al. Nature of the band gap of In_2O_3 revealed by first-principles calculations and x-ray spectroscopy. *Phys. Rev. Lett.* **2008**, *100*, No. 167402.
(6) Zhang, K. H. L.; Lazarov, V. K.; Galindo, P. L.; et al. Domain Matching Epitaxial Growth of In_2O_3 Thin Films on α-Al_2O_3(0001). *Cryst. Growth Des.* **2012**, *12*, 1000−1007.
(7) Bierwagen, O. Indium oxide-A transparent, wide-band gap semiconductor for (opto)electronic applications. *Semicond. Sci. Technol.* **2015**, *30*, No. 024001.
(8) Granqvist, C. G.; Hultåker, A. Transparent and conducting ITO films: new developments and applications. *Thin Solid Films* **2002**, *411*, 1−5.
(9) Zhang, J.; Shi, J.; Qi, D. C.; et al. Recent progress on the electronic structure, defect, and doping properties of Ga_2O_3. *APL Mater.* **2020**, *8*, No. 020906.
(10) Green, A. J.; Speck, J.; Xing, G.; et al. β-Gallium oxide power electronics. *APL Mater.* **2022**, *10*, No. 029201.
(11) Kaur, D.; Kumar, M. A Strategic review on gallium oxide based deep-ultraviolet photodetectors: Recent progress and future prospects. *Adv. Opt. Mater.* **2021**, *9*, No. 2002160.
(12) Zhang, J.; Willis, J.; Yang, Z.; et al. Deep UV transparent conductive oxide thin films realized through degenerately doped wide-bandgap gallium oxide. *Cell Rep. Phys. Sci.* **2022**, *3*, No. 100801.
(13) Peelaers, H.; Steiauf, D.; Varley, J. B.; et al. $(In_xGa_{1-x})_2O_3$ alloys for transparent electronics. *Phys. Rev. B* **2015**, *92*, No. 085206.
(14) Chen, W.; Xu, X.; Zhang, J.; et al. $(In_xGa_{1-x})_2O_3$ thin film based solar-blind deep UV photodetectors with ultra-high detectivity and on/off current ratio. *Adv. Opt. Mater.* **2022**, *10*, No. 2102138.
(15) Edwards, D. D.; Folkins, P. E.; Mason, T. O. Phase equilibria in the Ga_2O_3-In_2O_3 system. *J. Am. Ceram. Soc.* **1997**, *80*, 253−257.
(16) Oshima, T.; Fujita, S. Properties of Ga_2O_3-based $(In_xGa_{1-x})_2O_3$ alloy thin films grown by molecular beam epitaxy. *Phys. Status Solidi C* **2008**, *5*, 3113−3115.
(17) Swallow, J. E. N.; Palgrave, R. G.; Murgatroyd, P. A.; et al. Indium gallium oxide alloys: Electronic structure, optical gap, surface space charge, and chemical trends within common-cation semiconductors. *ACS Appl. Mater. Interfaces* **2021**, *13*, 2807−2819.
(18) Kranert, C.; Lenzner, J.; Jenderka, M.; et al. Lattice parameters and Raman-active phonon modes of $(In_xGa_{1-x})_2O_3$ for $x < 0.4$. *J. Appl. Phys.* **2014**, *116*, No. 013505.
(19) Chen, Y.; Liang, H.; Xia, X.; et al. The lattice distortion of β-Ga_2O_3 film grown on c-plane sapphire. *J. Mater. Sci. Mater. Electron.* **2015**, *26*, 3231−3235.
(20) Zhang, F. B.; Saito, K.; Tanaka, T.; et al. Structural and optical properties of Ga_2O_3 films on sapphire substrates by pulsed laser deposition. *J. Cryst. Growth* **2014**, *387*, 96−100.
(21) Matsuzaki, K.; Yanagi, H.; Kamiya, T.; et al. Field-induced current modulation in epitaxial film of deep-ultraviolet transparent oxide semiconductor Ga_2O_3. *Appl. Phys. Lett.* **2006**, *88*, No. 092106.
(22) Nakagomi, S.; Kokubun, Y. Crystal orientation of β-Ga_2O_3 thin films formed on c-plane and a-plane sapphire substrate. *J. Cryst. Growth* **2012**, *349*, 12−18.
(23) Wakabayashi, R.; Yoshimatsu, K.; Hattori, M.; Ohtomo, A. Epitaxial structure and electronic property of β-Ga_2O_3 films grown on MgO (100) substrates by pulsed-laser deposition. *Appl. Phys. Lett.* **2017**, *111*, No. 162101.
(24) Guo, D.; Wu, Z.; Li, P.; et al. Fabrication of β-Ga_2O_3 thin films and solar-blind photodetectors by laser MBE technology. *Opt. Mater. Express* **2014**, *4*, 1067−1076.
(25) Seiler, W.; Nistor, M.; Hebert, C.; Perrière, J. Epitaxial undoped indium oxide thin films: Structural and physical properties. *Sol. Energy Mater. Sol. Cells* **2013**, *116*, 34−42.
(26) Furthmüller, J.; Bechstedt, F. Quasiparticle bands and spectra of Ga_2O_3 polymorphs. *Phys. Rev. B* **2016**, *93*, No. 115204.
(27) Li, G. L.; Zhang, F.; Cui, Y. T.; et al. Electronic structure of β-Ga_2O_3 single crystals investigated by hard x-ray photoelectron spectroscopy. *Appl. Phys. Lett.* **2015**, *107*, No. 022109.
(28) Körber, C.; Krishnakumar, V.; Klein, A.; et al. Electronic structure of In_2O_3 and Sn-doped In_2O_3 by hard x-ray photoemission spectroscopy. *Phys. Rev. B* **2010**, *81*, No. 165207.
(29) Erhart, P.; Klein, A.; Egdell, R. G.; Albe, K. Band structure of indium oxide: indirect versus direct band gap. *Phys. Rev. B* **2007**, *75*, No. 153205.
(30) Zhang, K. H. L.; Egdell, R. G.; Offi, F.; et al. Microscopic origin of electron accumulation in In_2O_3. *Phys. Rev. Lett.* **2013**, *110*, No. 056803.
(31) Davies, D. W.; Walsh, A.; Mudd, J. J.; et al. Identification of lone-pair surface states on indium oxide. *J. Phys. Chem. C* **2019**, *123*, 1700−1709.
(32) King, P. D. C.; Veal, T. D.; Fuchs, F.; et al. Band gap, electronic structure, and surface electron accumulation of cubic and rhombohedral In_2O_3. *Phys. Rev. B* **2009**, *79*, No. 205211.
(33) Jovic, V.; Moser, S.; Papadogianni, A.; et al. The itinerant 2D electron gas of the indium oxide (111) surface: implications for carbon- and energy-conversion applications. *Small* **2020**, *16*, No. 1903321.
(34) Michel, J.; Splith, D.; Rombach, J.; et al. Processing strategies for high-performance Schottky contacts on n-type oxide semiconductors: insights from In_2O_3. *ACS Appl. Mater. Interfaces* **2019**, *11*, 27073−27087.
(35) Swallow, J. E. N.; Varley, J. B.; Jones, L. A. H.; et al. Transition from electron accumulation to depletion at β-Ga_2O_3 surfaces: The role of hydrogen and the charge neutrality level. *APL Mater.* **2019**, *7*, No. 022528.
(36) Navarro-Quezada, A.; Alamé, S.; Esser, N.; et al. Near valence-band electronic properties of semiconducting β−Ga_2O_3(100) single crystals. *Phys. Rev. B* **2015**, *92*, No. 195306.

Recommended by ACS

Exploiting the Nanostructural Anisotropy of β-Ga_2O_3 to Demonstrate Giant Improvement in Titanium/Gold Ohmic Contacts

Ming-Hsun Lee, Rebecca L. Peterson, *et al.*
AUGUST 09, 2022
ACS NANO
READ

Computational Prediction and Experimental Realization of Earth-Abundant Transparent Conducting Oxide Ga-Doped $ZnSb_2O_6$

Adam J. Jackson, David O. Scanlon, *et al.*
OCTOBER 10, 2022
ACS ENERGY LETTERS
READ

Spatially Resolved Investigation of the Bandgap Variation across a β-$(Al_xGa_{1-x})_2O_3$/β-Ga_2O_3 Interface by STEM–VEELS

Adrian Chmielewski, Nasim Alem, *et al.*
JANUARY 23, 2022
ACS APPLIED ELECTRONIC MATERIALS
READ

Controllable Ga/Ga_2O_3 Nanowire Growth at High Temperatures Enabled by Au and Pd Quantum Dot Catalysts

Hang Wang, Yunfa Chen, *et al.*
SEPTEMBER 15, 2022
CRYSTAL GROWTH & DESIGN
READ

Get More Suggestions >

https://doi.org/10.1021/acs.cgd.2c00948
Cryst. Growth Des. 2022, 22, 7325−7330